AD NUMBER

AD874029

LIMITATION CHANGES

TO:

Approved for public release; distribution is unlimited.

FROM:

Distribution authorized to U.S. Gov't. agencies and their contractors; Critical Technology; APR 1970. Other requests shall be referred to U.S. Army Aviation Materiel Laboratories, Fort Eustist Virginia 23604. This document contains export-controlled technical data.

AUTHORITY

USAAMRDL ltr, 18 Jun 1971

AD 20

USAAVLABS TECHNICAL REPORT 70-25

FLUIDIC VORTEX ANGULAR RATE SENSOR CONCEPT INVESTIGATION FOR HELICOPTERS AND V/STOL AIRCRAFT

By

G. P. Wachtell

April 1970

U. S. ARMY AVIATION MATERIEL LABORATORIES
FORT EUSTIS, VIRGINIA

CONTRACT DAAJ02-69-C-0010
THE FRANKLIN INSTITUTE RESEARCH LABORATORIES
PHILADELPHIA, PENNSYLVANIA

DEPARTMENT OF THE ARMY
HEADQUARTERS US ARMY AVIATION MATERIEL LABORATORIES
FORT EUSTIS, VIRGINIA 23604

This report has been reviewed by the U. S. Army Aviation Materiel Laboratories and is considered to be technically sound. The report is published for the exchange of information and consideration in future related programs.

Task 1F162203A14186
Contract DAAJ02-69-C-0010
USAAVLABS Technical Report 70-25
April 1970

FLUIDIC VORTEX ANGULAR RATE SENSOR CONCEPT INVESTIGATION FOR HELICOPTERS AND V/STOL AIRCRAFT

Final Report

By

G. P. Wachtell

Prepared by

The Franklin Institute Research Laboratories
Philadelphia, Pennsylvania

for

U. S. ARMY AVIATION MATERIEL LABORATORIES
FORT EUSTIS, VIRGINIA

ABSTRACT

An experimental investigation was undertaken to establish the feasibility of fluidic vortex angular rate sensor concepts for application in helicopter and V/STOL aircraft stability augmentation systems.

Theories of various possible rate sensing devices based on rapid vortex flows are presented, with experimental demonstration of the principle of one in which the swirl flow axis lags behind the chamber axis when the chamber is rotated about a line perpendicular to its axis. Two modifications yielded sensitivities less than ultimately desired, by factors on the order of 2000 and 200. Observations on the flow pattern in jets emerging from a pair of concentric vortex chambers showed that the concept of the vortex axis jet angular rate sensor (VAJARS) discussed theoretically in a previous feasibility study would have to overcome problems created by turbulence and flow reversal along the axis. An attempt was made to demonstrate a device of high theoretical sensitivity, in which a cylindrical core supported on an axis perpendicular to the core axis is subjected to a torque due to the pressure gradient generated in an annular passage by Coriolis forces. Noise due to turbulence, as well as instability in the position of the core, was a problem that is believed to be possible to overcome.

Theoretical discussions are also given of a gyroscope in which the fluid stream is the rotor, and of the deflection of the jet emerging from a swirl chamber subjected to an angular rate. A flow rate sensor based on the iodine-iodide redox system was demonstrated, in an attempt to develop a velocity probe. Sensitivity was an order of magnitude too high for the present flow studies.

BLANK PAGE

TABLE OF CONTENTS

LIST OF ILLUSTRATIONS

LIST OF SYMBOLS

A_d	total disc area, ft^2
A_s	total swirl chamber end face area, ft^2
c	concentration of I_3^- ions, per ft^3
D	diffusion constant, ft^2/sec
g	acceleration of gravity, ft/sec^2
$\underline{i}$, $\underline{j}$, $\underline{k}$, $\underline{n}$	unit vectors in x, y, z, and stream directions
L	length of chamber, ft
L'	distance from swirl chamber exit orifice to pressure sensors, ft
P	pressure, lb/ft^2
ΔP	pressure difference, lb/ft^2
P_1, P_2	pressures at locations 1 and 2, lb/ft^2
$P(\theta,x)$	pressure on cylindrical core at coordinates (θ,x), lb/ft^2
$\underline{P}$	angular momentum vector, ft-lb-sec
P_x, P_y	angular momentum components about x and y axes, ft-lb-sec
Q	volumetric flow rate, ft^3/sec
r	radial coordinate, ft
R	radius of chamber, ft
ΔR	radial clearance between housing and cylindrical core, ft
Re	Reynolds number, $\rho ur/\mu$, dimensionless
s	displacement of swirl flow axis, ft
T_c	torque due to Coriolis forces, ft-lb
T_{cyl}	torque on cylindrical core, ft-lb
T_h	torque on housing, ft-lb
T_o	magnitude of flow rate of angular momentum of outflowing stream due to its own rotation, ft-lb

T_y	torque about y axis, ft-lb
T_{yd}	T_y applied to discs, ft-lb
t	time, sec
u	radially inward component of velocity, ft/sec
v	circumferential component of velocity, ft/sec
v_R	v for r = R, ft/sec
V	chamber volume, ft^3
V_R	inlet velocity, ft/sec
W	speed of outflowing stream, ft/sec
x,y,z	coordinate system axes
x	chamber axis
z	axis of rotation
θ	angle between swirl flow axis and chamber axis, deg
θ	angular coordinate, deg
μ	viscosity, lb/ft-sec
ρ	fluid density, lb/ft^3
τ	V/Q, sec
τ'	L'/W, sec
Ω	angular velocity of chamber, radians/sec
Underline	vector
Subscript c	Coriolis

INTRODUCTION

This report gives the results of a feasibility and experimental study of the vortex axis jet angular rate sensor.

The need for an angular rate sensor arises in connection with fluidic stability augmentation systems for helicopters and V/STOL aircraft. As a guideline, it was assumed that variations in the angular rate at frequencies up to 10 cps have to be detected, and that the sensitivity sought for the rate sensor is 0.05 deg/sec.

VAJARS CONCEPT

The principle of the vortex axis jet angular rate sensor (VAJARS) concept is illustrated in Figure 1. A straight small-diameter vortex is provided along the axis of a large-diameter jet, which protects the vortex from disturbances due to entrainment of the surrounding quiescent fluid. The vortex passes between a pair of sensing elements that are placed in the potential flow field just outside the vortex core.

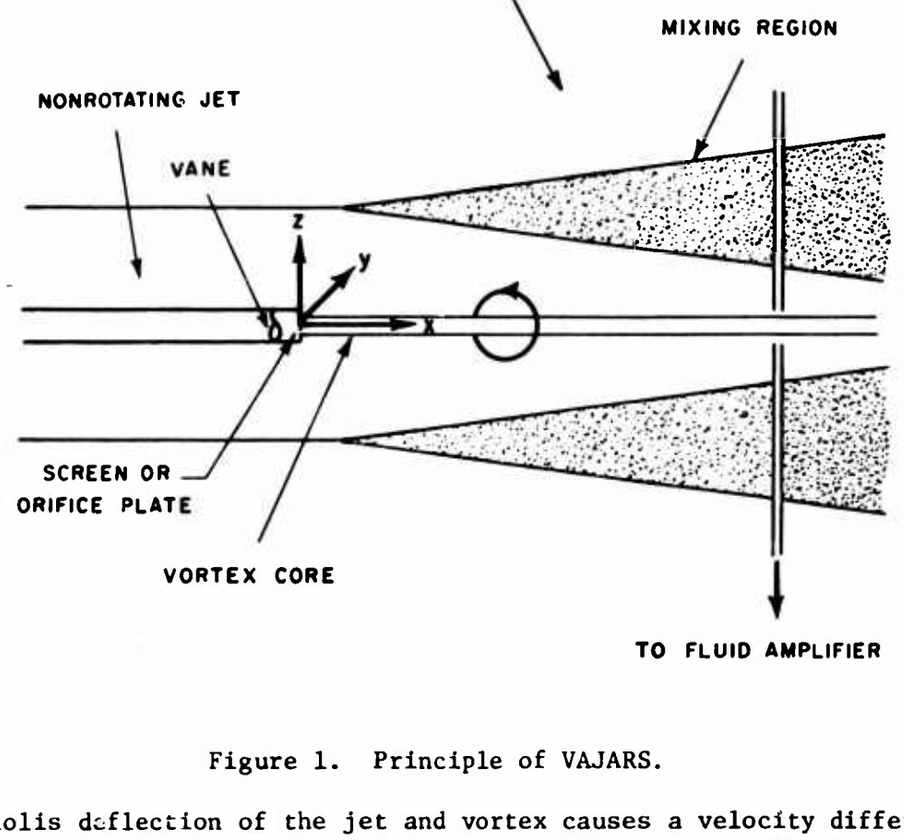

Figure 1. Principle of VAJARS.

Coriolis deflection of the jet and vortex causes a velocity differential at the sensing elements. Possible sensing elements are fluid amplifier control ports or hot-wire anemometer probes. An intended advantage over the ordinary jet-type rate sensor is that the rotational velocity can be made much higher than the linear drift velocity, leading theoretically to higher sensitivity.

EXPERIMENTAL ARRANGEMENT

Preliminary experiments were performed in a rectangular aluminum test tank that was 2 feet wide, 2 feet deep, and 6 feet long. One 6-foot-long face was of Plexiglas, permitting flow visualization.

Figure 2 shows the concentric vortex chambers used in the preliminary experiments and Figure 3 shows the major component parts. Part (a) has an inner groove into which part (c) fits. Nonrotating flow can enter from under the deflecting plate at the center of part (a). Flow entering between the two grooves of part (a) goes through the slots in part (c) to produce rotation in the flow emerging from the tube of part (d). Part (d) fits into the outer groove of part (b), thus dividing part (a) into two plenums, the outer one supplying the flow for part (b). In addition to four holes that admit nonrotating flow to part (b), part (a) also has provision for tangential inlet flows with a choice of rotation in either direction. As an indication of size, the external tube in part (b) projects 5-1/2 inches.

The vortex chamber apparatus was supported in the test tank with the chamber axis horizontal, so that the chamber could be rotated manually about a vertical axis. For most of the preliminary observations, the chamber was submerged. For a few observations, the water level in the test tank was lowered so that the chamber was not submerged. Water was pumped into the vortex chamber inlets and out of the test tank.

Flow visualization was accomplished in three ways:

1. The entire system contained phenolphthalein solution, an acid-base indicator that is red in alkaline solutions and colorless in neutral or acid solutions. The inlet water for the axial jet was saturated with calcium hydroxide, and was therefore red. The water in the tank was neutral or slightly acidified with hydrochloric acid. The red axial jet was clearly visible, and disappeared as it mixed with the surrounding fluid.
2. Air bubbles entrained in the outer jet gave a visual indication of flow.
3. A short length of thread on the end of a needle gave an indication of the direction of the flow velocity at any point in the jet after it entered the tank.

One version of the vortex chamber had pressure-sensing ports which were connected to manometers.

A simple rate table was constructed with two levels. The lower level supported the water pump, and the upper level shown in Figure 4 supported the device under test as well as a surge tank. In some observations, the air pressure above the water in the surge tank was varied. The rate table is reversible, and its minimum speed is about ten times the 0.05

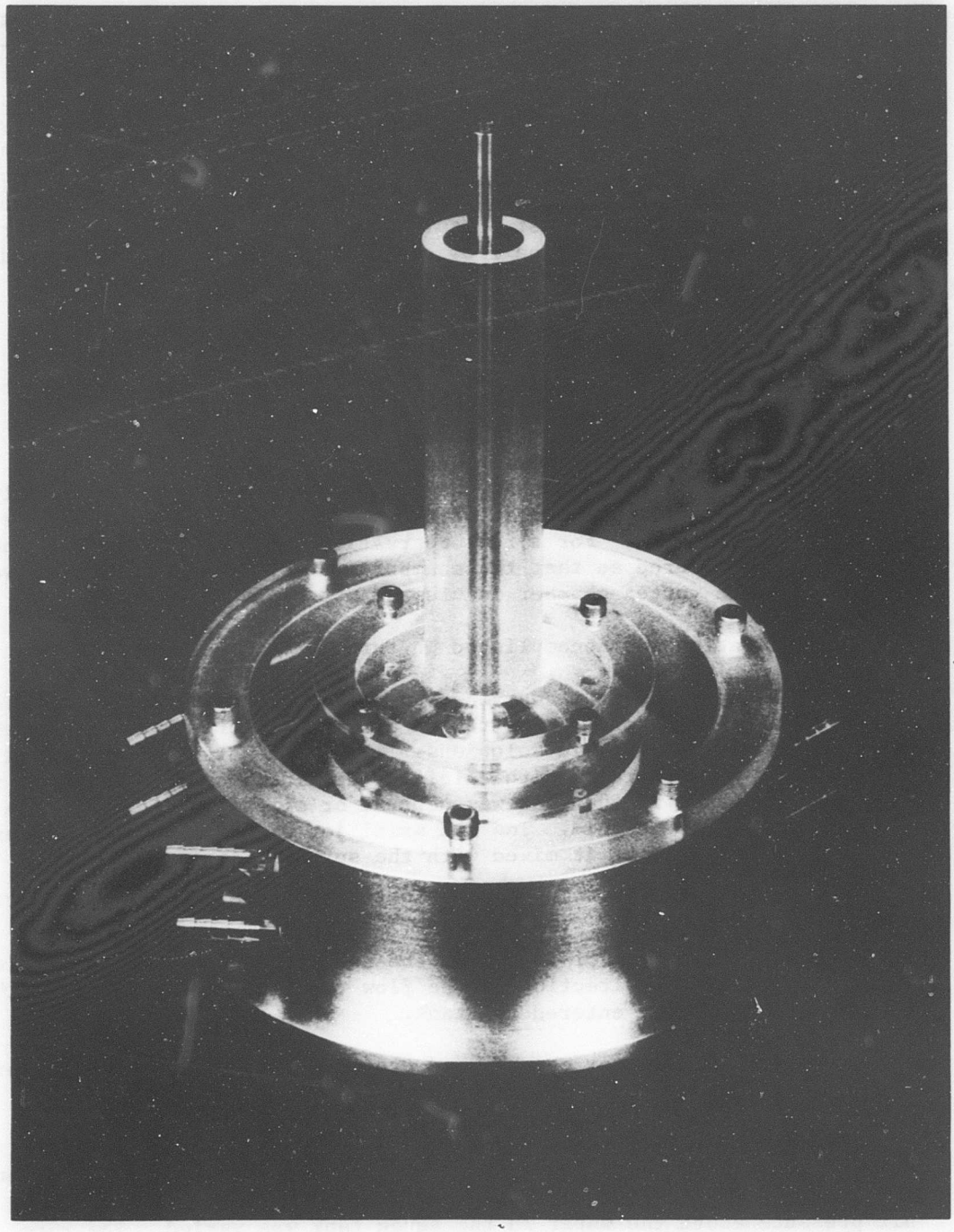

Figure 2. Concentric Vortex Chambers.

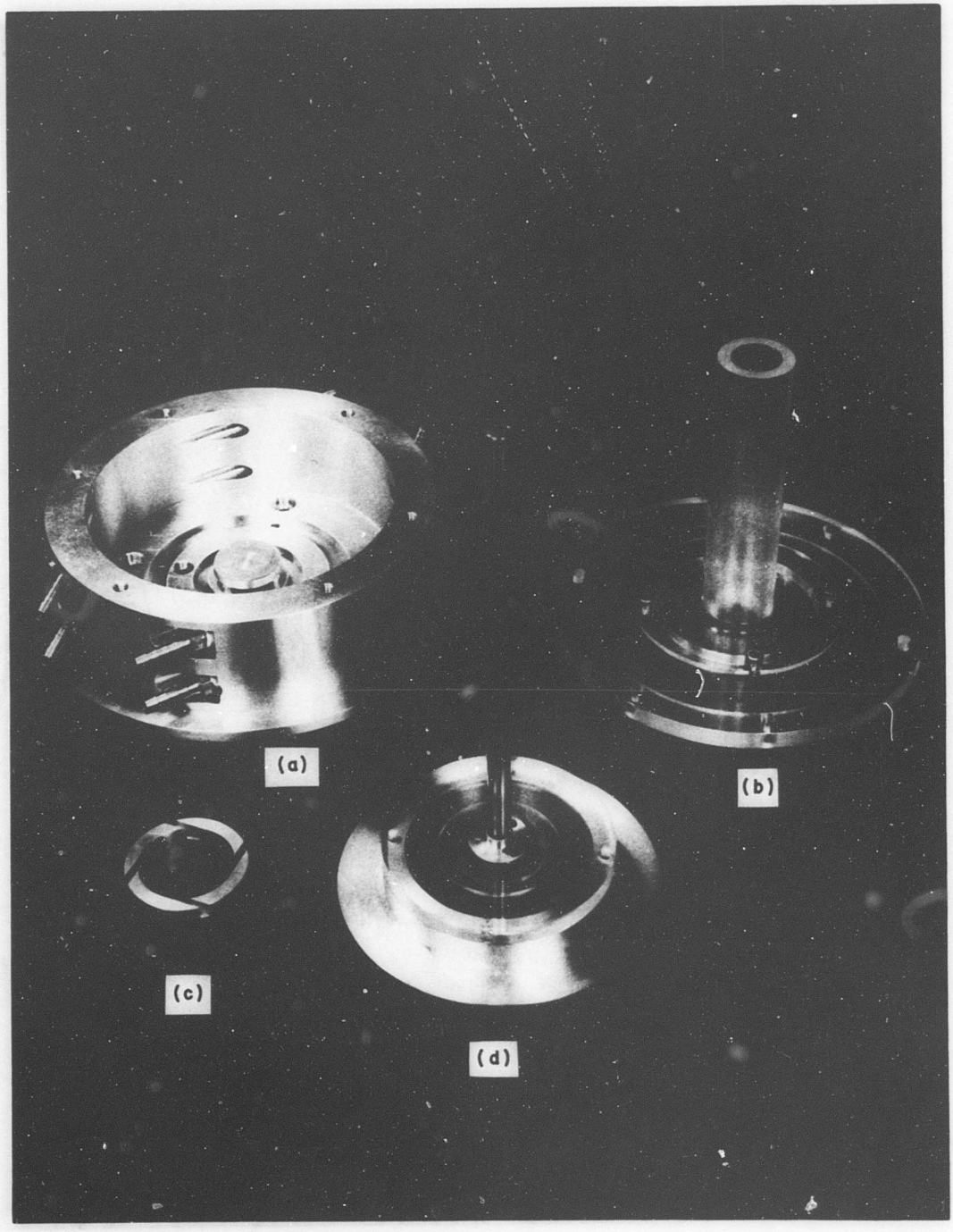

Figure 3. Component Parts of Concentric Vortex Chambers.

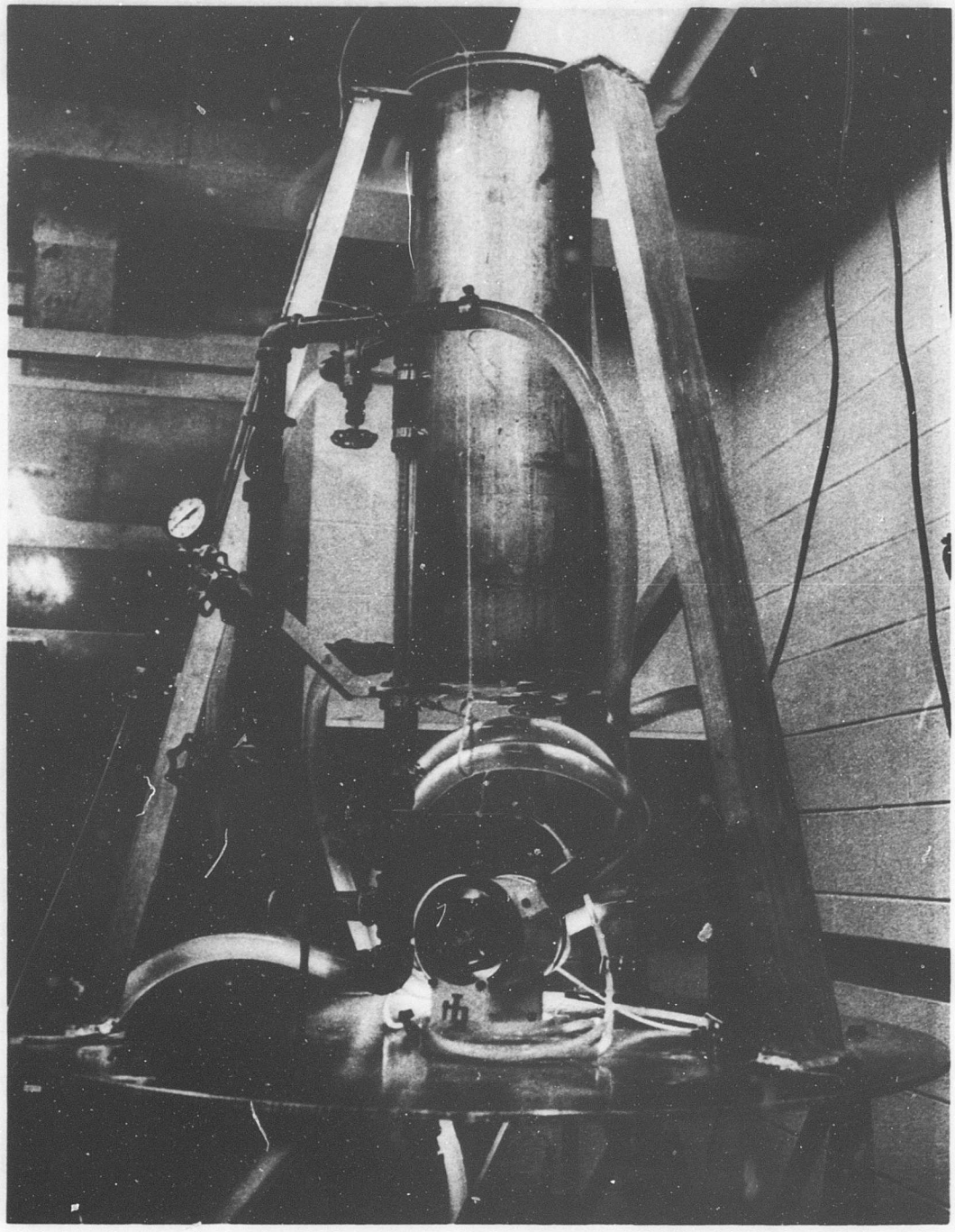

Figure 4. Upper Level of Rate Table.

deg/sec rate which is ultimately desired. The reason for this was that the immediate objective was to demonstrate a principle of operation. For some tests, a pressure transducer was connected to one output port of the device under test and signals were displayed by means of a strip chart recorder.

IODINE VELOCITY PROBE

It was thought that a velocity probe based on the iodine-iodide redox system would be useful in the VAJARS study. By using a suitable solution as the fluid, an electrical current would be observed that is a calibrated function of the flow velocity past the probe.

The following experiment, for which background information is given in Reference 2, was performed by P. M. W. Nave. The electrolytic solution contained 0.05 n KI and 0.001 n I_2. Figure 5 shows the experimental arrangement, and Figure 6 shows the calibration curve that was obtained. The presence of an electrical current with zero flow velocity is consistent with the following theory:

Provided the applied potential stays below the decomposition potential of water ($\sim$1.0 V), only the following reaction can take place:

$$I_3^- + 2e \rightleftarrows 3I^-$$

Since there are many more I^- ions available than I_3^- ions, the cathodic reaction is the current limiting process. In the absence of convective flow, the diffusion of I_3^- is rate determining because the current is proportional to $D\,\partial c/\partial x$, where D is the diffusion constant and c is the concentration of I_3^-. The steady-state current in the absence of flow is determined by the distance between the two electrodes. If a fairly strong flow is suddenly shut off, the approximately spherical diffusion about the small cathode determines an average $\partial c/\partial x$ and thus the zero flow current. The zero flow current given in Figure 6 should be understood in this sense.

The measurements were taken with a graduated cylinder and a stop watch. Measured liquid volumes were between 15 and 20 ml.

The flow velocities that could be detected were an order of magnitude smaller than the velocities of interest for present purposes. Although there are other applications for which a further development would be of value, effort under the current project was discontinued.

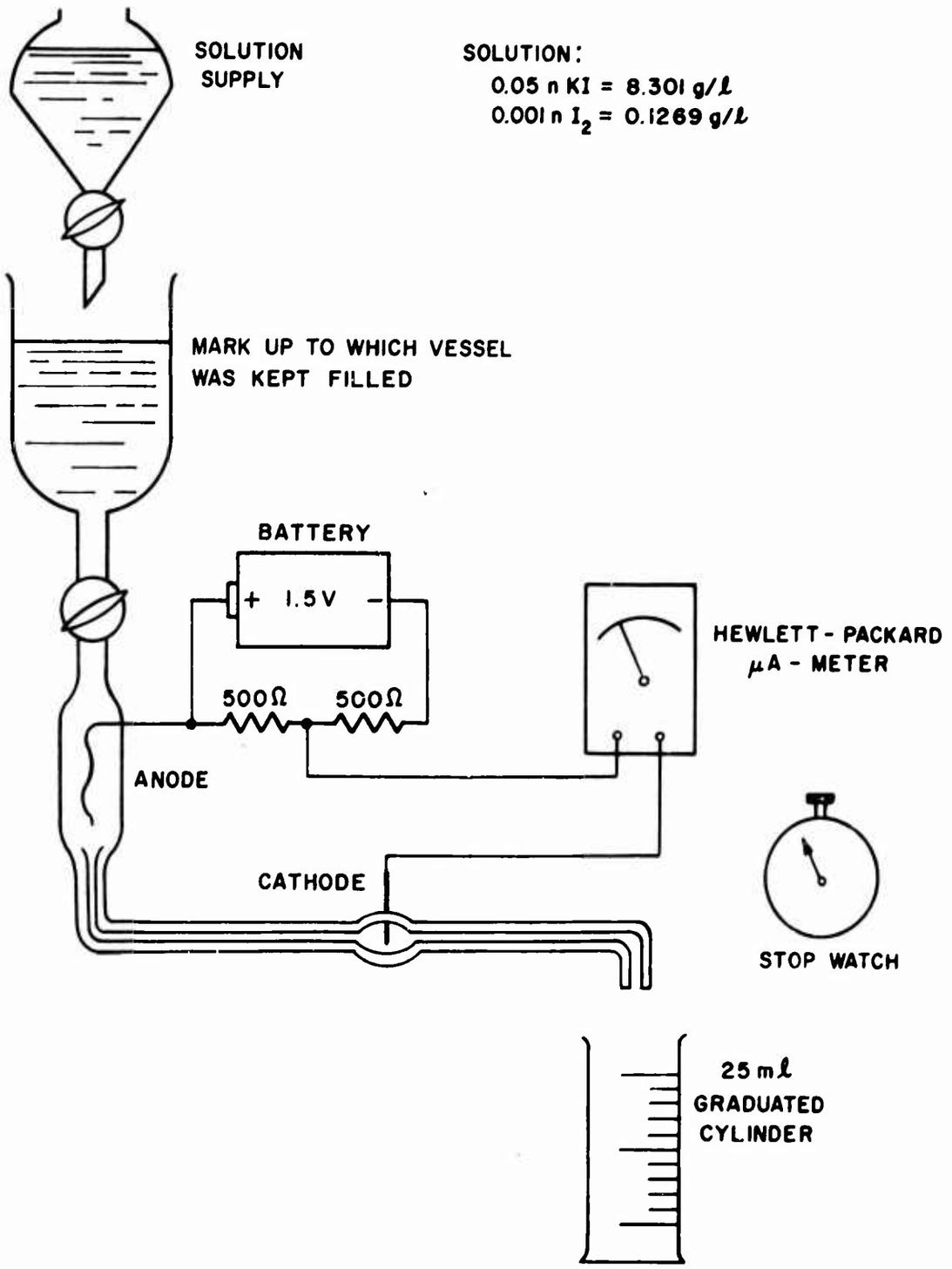

Figure 5. Electrolytic Flowmeter.

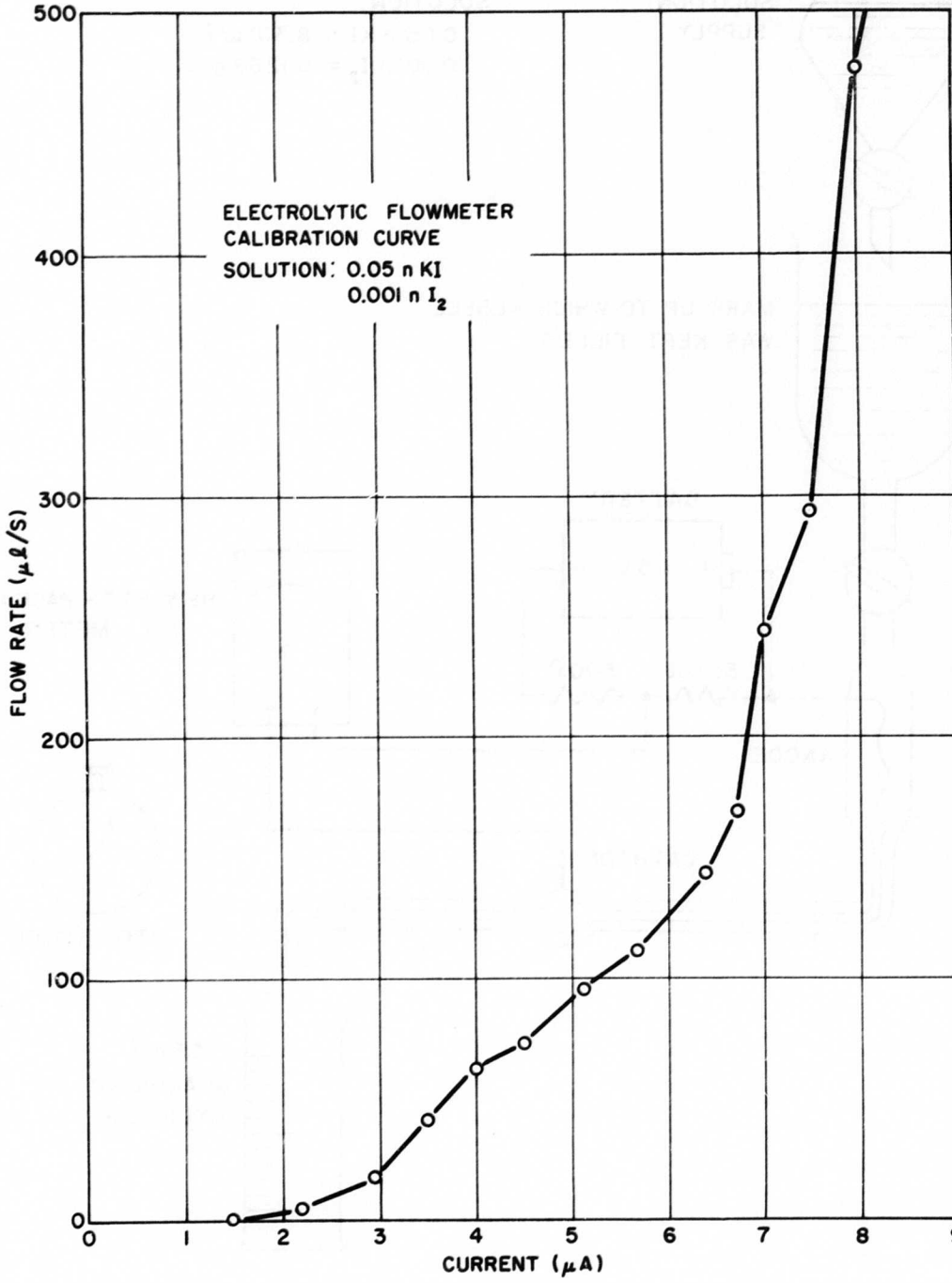

Figure 6. Electrolytic Flowmeter Calibration.

OBSERVATIONS WITH CONCENTRIC VORTEX CHAMBERS

Various observations were made in which the variables included axial and outer jet flow rates and rotation rates. The results are summarized as follows:

1. When the jet was not submerged (i.e., when the water level in the tank was low) and the outer jet was rotated, centrifugal force caused the jet to fan out over a conical surface as the jet emerged.
2. With or without rotation of the submerged outer jet, the axial jet mixed rapidly with the surrounding fluid.
3. The axial velocity of the axial jet exceeded its rotational velocity, indicating the need to modify the method of producing rotation. The outer jet could be made to rotate much more strongly, indicating that the required modification is possible.

The blunt end of the plastic tube from which the outer jet emerged was thought to create a turbulent wake. The end of the tube was therefore tapered.

The parts for generating the axial flow were removed, in order to study the outer jet alone. A hypodermic tube along the axis was used to inject red alkaline solution. Axial fluid rapidly mixed with the rotating jet. Furthermore, rotation of the jet caused a local flow reversal along the axis near the end of the plastic tube, as indicated by air bubbles trapped along the axis by the combination of the reversed flow and centrifugal forces.

A tube, connected to the outlet of the tank, was supported coaxially with the jet and held at various distances from the end of the plastic tube. When the movable exhaust tube was held sufficiently close to the plastic tube, air bubbles were no longer trapped along the axis of the rotating flow. This was the expected result, and is explained by the fact that flow reversal (due to low pressure along the axis as a result of centrifugal forces) was prevented. Furthermore, air bubbles fed into the stream near the axis remained near the axis, indicating that severe mixing did not occur inside the plastic tube.

As a result of these observations, attention shifted from the external jet flow to flow internal to the plastic tube, leading to the concept of the swirl chamber discussed in the following section.

THEORY OF SWIRL CHAMBER RATE SENSOR

Consider a cylindrical chamber with tangential inlet flow. Exhaust is through an axially located hole in one end plate. The hole is small enough so that sufficient pressure is maintained in the chamber to avoid cavitation.

Ignoring the axial component of the flow, and also ignoring boundary-layer effects on the second end plate (exhaust being through the first end plate) as well as shear forces between successive cylindrical layers of flow, the swirl flow will be characterized by extremely high circumferential velocity near its axis, since v is proportional to 1/r.

Let the chamber axis be the x axis, and let the z axis be vertical. If the chamber is rotated about the z axis, starting from rest at time zero, the swirl flow axis will become rotated in the xy plane, making a small angle with the chamber axis. Let Ω be the angular velocity of the chamber about the z axis, V be the chamber volume, and Q be the volumetric flow rate. The angle between the swirl flow axis and the chamber axis will be on the order of $\theta = \Omega\tau$, where $\tau = V/Q$ is the time required to replace all the fluid in the chamber with fresh fluid. Assuming that the swirl flow axis crosses the chamber axis at the center of the chamber, the swirl flow axis will be displaced horizontally along the second end plate by

$$s = \frac{\theta L}{2} = \frac{\Omega V L}{2Q} \tag{1}$$

where L is the length of the chamber.

If pressure sensing ports are located at $y = \pm r$ on the second end plate, a pressure difference ΔP will be obtained between them, since the pressure at one will rise and at the other will fall by the amount $s(dP/dr)$, so that

$$\Delta P = 2s \left|\frac{dP}{dr}\right| \tag{2}$$

Since $v = (v_R)R/r$, where v_R is v at radius R, we have

$$\frac{dP}{dr} = \frac{d}{dr}\left(\frac{\rho v^2}{2g}\right) = \frac{\rho}{2g} v_R^2 R^2 \frac{d}{dr}\left(\frac{1}{r^2}\right) = -\frac{\rho}{g}\frac{v_R^2 R^2}{r^3} \tag{3}$$

$$\Delta P = \frac{2\rho v_R^2 R^2 s}{g r^3} = \frac{\rho v_R^2 R^2 \Omega V L}{g r^3 Q} \tag{4}$$

Assuming the following values, $\rho = 50$ lb/ft^3, $v_R = 6$ ft/sec, $R = 0.1$ ft, $\Omega = 0.05$ deg/sec $= 0.87 \times 10^{-3}$ rad/sec, $L = 0.5$ ft, $Q = 0.15$ ft^3/sec, and $r = 5 \times 10^{-3}$ ft (separation between pressure taps = approx. 1/8 in.), we obtain the following results:

$$v = 0.0157 \text{ ft}^3, \ \tau = 0.105 \text{ sec, and } \Delta P = 1.4 \text{ psi.} \tag{5}$$

τ represents a tolerable time lag and ΔP is an easily detected pressure difference.

The foregoing theory neglects the effect of shear on the flow pattern. The following analysis shows that for sufficiently high Reynolds number, the effect of shear on a two-dimensional swirl flow is negligible. Although the analysis does not take account of boundary-layer effects at the end plates, or the effect of axial flow components, the result encouraged construction of an experimental swirl chamber.

With cylindrical polar coordinates, consider a section of the cylindrical chamber with one unit of length in the z direction. Let u and v be radially inward and tangential velocity components, respectively.

For the region within the circle of radius r, there is an inflow of angular momentum from two sources:

1. Convective inflow at the rate (mass flow rate).(Angular momentum per unit pass)
$$= (\rho Q)\ (rv) \tag{6}$$
where $Q = 2\pi ru$ = total volumetric flow rate (per unit of z). (7)
2. Torque due to shear = (total shear force)$\cdot$ (Lever arm) (8)

The shear rate would be zero between layers at r and r + dr if dv were equal to dv_o, where

$$\frac{v+dv_o}{r+dr} = \frac{v}{r} \tag{9}$$

The shear rate is therefore

$$\frac{dv-dv_o}{dr} = \frac{dv}{dr} - \frac{dv_o}{dr} = \frac{dv}{dr} - \frac{v}{r} = r\,\frac{d}{dr}\left(\frac{v}{r}\right) \tag{10}$$

Multiplying by $2\pi r\mu$ to obtain the total shear force around the circumference at radius r, and noting that the lever arm equals r, we find the torque to be

$$2\pi\mu r^3\,\frac{d}{dr}\left(\frac{v}{r}\right)$$

Since the angular momentum in the region between any two radii r_1 and r_2 is constant, the inflow of angular momentum is independent of r:

$$\rho Q\dot{r}v + 2\pi\mu\, r^3 \frac{d}{dr}\left(\frac{v}{r}\right) = C \tag{11}$$

The solution of this equation is

$$rv = A_1 r^{2-Re} + \frac{A_2}{Re-2} \tag{12}$$

where $Re = \rho ur/\mu$ is the Reynolds number expressed in terms of the radial velocity component, and

$A_2 = C/(2\pi\mu)$.

Since $Re = \rho Q/(2\pi\mu)$, Re is independent of r.

If $v = v_R$ for $r = R$ (large radius, where flow is injected) and $v = v_o$ for $r = r_o$ (small radius, where exit conditions may affect v), we may express the result as follows:

$$rv = Rv_R\left[1 + \frac{1 - \left(\frac{r}{R}\right)^{Re-2}}{\left(\frac{r}{R}\right)^{Re-2} - \left(\frac{r}{r_o}\right)^{Re-2}}\right] + r_o v_o\left[\frac{\left(\frac{r}{R}\right)^{Re-2} - 1}{\left(\frac{r}{R}\right)^{Re-2} - \left(\frac{r}{r_o}\right)^{Re-2}}\right] \tag{13}$$

For large Re and $R>r>r_o$, with r not too close to r_o, $rv = Rv_R$, approximately. That is, v has approximately the same value it would have in a nonviscous flow, and this is true even for small radii.

ALTERNATIVE PRINCIPLES

Several principles were thought of whereby fluidic rate sensors may be possible, utilizing rapidly rotating flows. These are grouped into two major categories:

I. With moving solid parts.

II. Without moving solid parts.

FLUIDIC RATE SENSORS WITH MOVING SOLID PARTS

In Category I, the moving solid parts move only a very short distance. Various designs are possible, and these may be subdivided into two groups:

Analogy to gyroscope.
Coriolis pressure gradient.

Analogy to Gyroscope

In a gyroscope, the rotor has angular momentum P_x about a horitontal axis (x-axis). A torque T_y about the horizontal y-axis constitutes a rate of change of P_y, and causes a precession about the vertical z-axis with the angular velocity

$$\Omega = T_y/P_x \tag{14}$$

The rotor is mounted in gimbals so that a torque T_z may be applied about the z-axis, causing precession about the y-axis. Torque T_z will occur if the gimbals are mounted in a rotating coordinate system which rotates about the z-axis. However, T_z will be reduced to zero if the rotor is made to precess about the z-axis with the same angular velocity. In a gyroscope, precession about the y-axis is detected and brought to zero by applying torque T_y that causes the required precession about the z-axis. The applied torque T_y is a measure of the angular rate Ω of the rotating coordinate system, in accordance with Equation (14).

An equivalent point of view that yields the same result is to consider the Coriolis force experienced by each small element of volume of the rotor. The net force (thrust) on the rotor is readily seen to be zero, but a net torque T_c is found about the y-axis. This torque, if left unbalanced, would cause a precession. The torque that must be applied to prevent precession is $T_y = - T_c$ and is given by Equation (14).

Equivalently, one may say that to an observer situated in the rotating coordinate system, it appears that Coriolis forces are supplying angular momentum at the rate

$$(\underline{T})_c = (d\underline{P}/dt)_c = \underline{P} \times \underline{\Omega} \qquad (15)$$

where $\underline{T}$, $\underline{P}$ and $\underline{\Omega}$ are vectors and the subscript c stands for Coriolis.

One may make a fluid gyroscope by replacing the gyroscope rotor by a tube with fluid flowing through it, as in Figure 7. The Coriolis force experienced by each element of fluid in the loop of tube is transmitted directly to the tube wall. The method of sensing T_c is not shown in Figure 7.

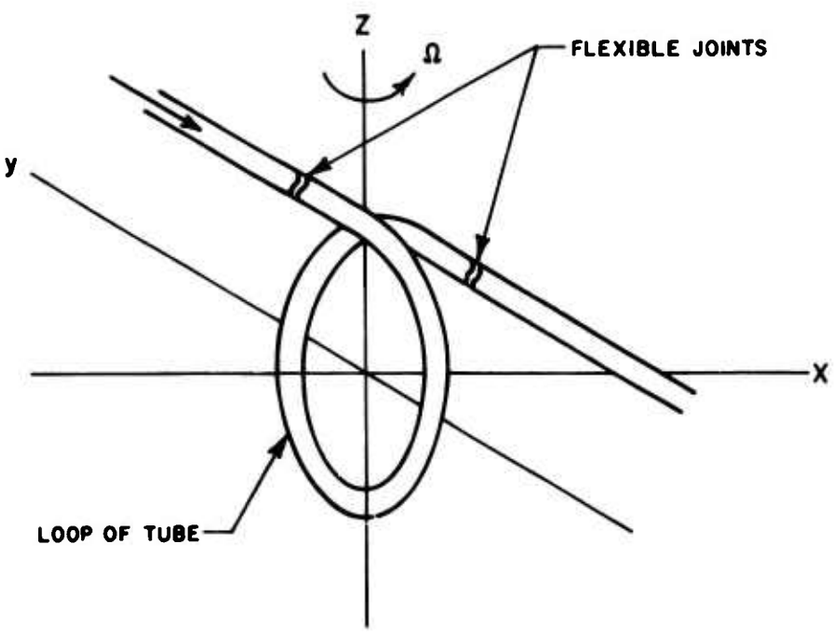

Figure 7. Fluid Analogy to Gyro Rotor.

The tube may be bent into a helix of several (say n) turns, instead of a single turn. The total angular momentum P_x is n times that in one turn, and the resulting torque is also n times as large, so that Equation (15) still holds.

Figure 8 shows a further development of the same principle. Fluid enters the plenum and passes through slots into the swirl chamber. Several discs are connected to each other by rods, forming a rigid assembly that can move inside the swirl chamber. Flow swirls inward in the spaces between the discs and then passes through the central holes in the discs to the

swirl chamber exit. Motion of the disc assembly (which constitutes the moving part) is limited by any of various means. In Figure 8, for example, the assembly is supported on a gimbal or pivot, so that it can rotate about the y-axis (perpendicular to the page). The sensors generate the torque T_y required to prevent rotation.

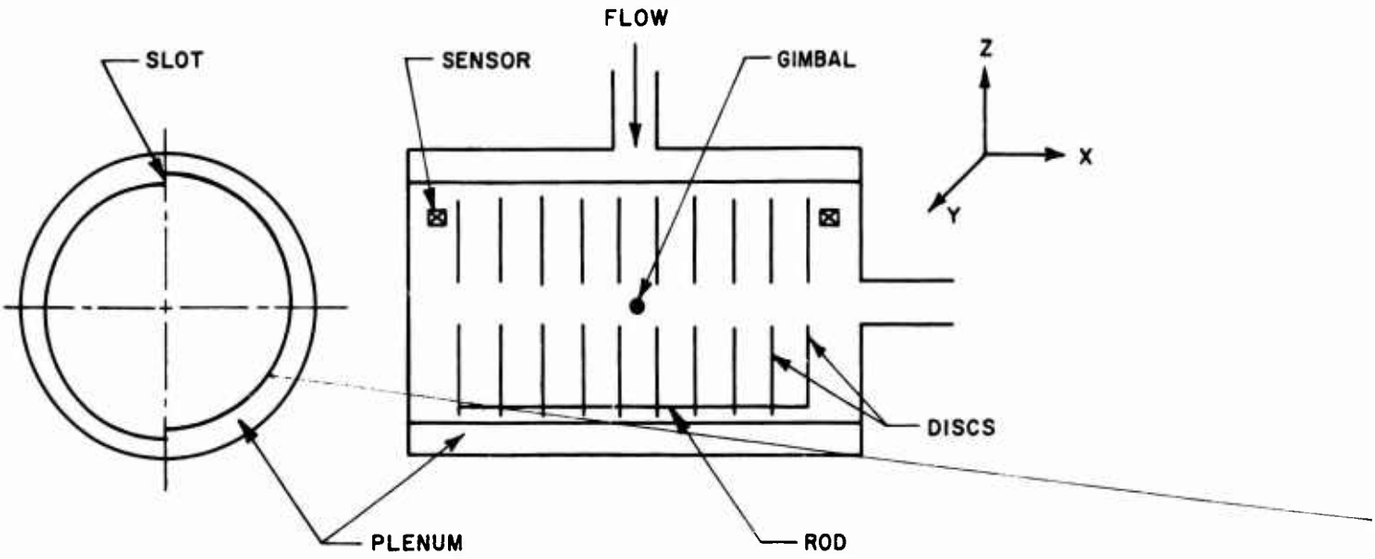

Figure 8. Swirl Flow Fluid Gyro.

Figure 9 shows a possible sensor arrangement for the swirl flow fluid gyro. Movement of the disc toward the sensor increases the pressure P_1 applied to sensor area A, generating a torque P_1AR about the y-axis. If pressure P_2 occurs in the other sensor, the torque applied to the discs is

$$T_{yd} = (P_1-P_2)AR \tag{16}$$

In Figure 8, T_c is transmitted by the fluid partly to the discs and partly to the end faces of the swirl chamber, the discs and the chamber end faces sharing T_c in proportion to their surface areas (counting both sides of each disc). If A_d and A_s are the total disc area and the total swirl chamber end face area, respectively,

$$T_{yd} = - T_c \frac{A_d}{A_d + A_s} \tag{17}$$

Thus, (P_1-P_2) is a measure of T_c and therefore of Ω.

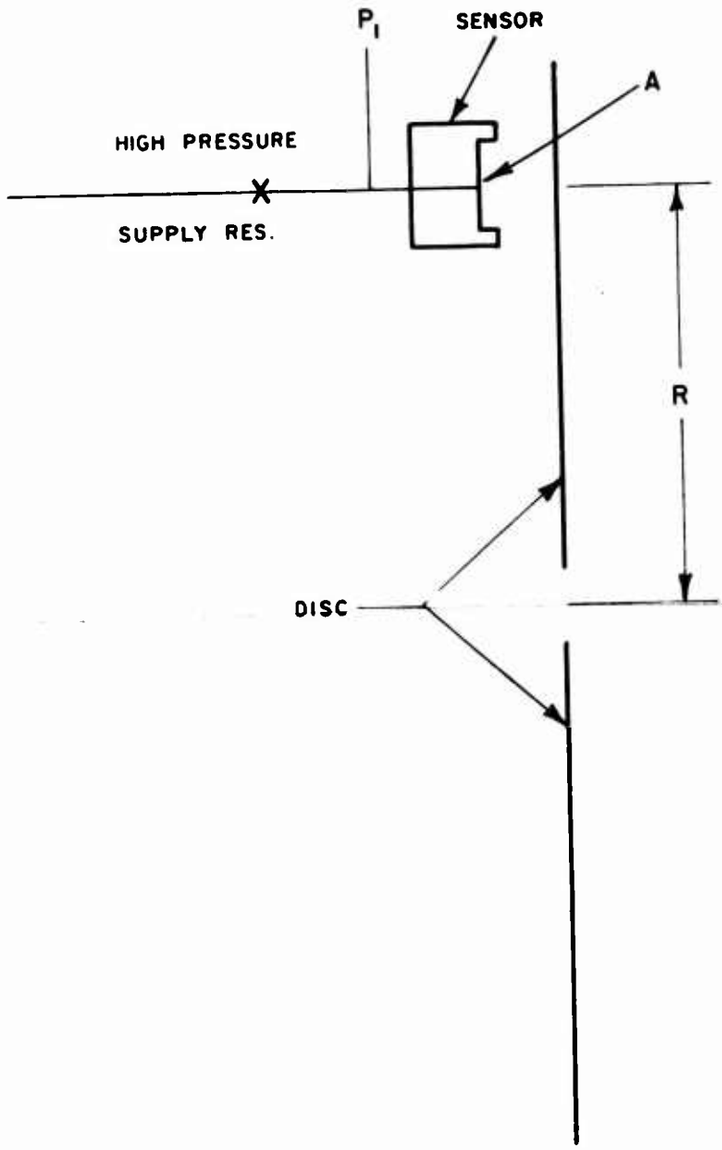

Figure 9. Torque Sensor.

The angular momentum that can be stored in the swirl chamber is comparable to that in a small gyroscope. Consequently, sensitivity approaching that of a gyro should be possible.

Coriolis Pressure Gradients Device

Since this device was briefly studied experimentally, its theory is given on page 23.

FLUIDIC RATE SENSORS WITHOUT MOVING SOLID PARTS

The concepts described above require only very small motions in the moving parts and appear in theory to be capable of practical development. Nevertheless, devices with no moving solid parts are attractive. Let Q be the volumetric flow rate through a swirl chamber of volume V in which angular momentum $\underline{P}$ is stored in the fluid. The flow rate of angular momentum into the chamber is $\underline{T}_{in}$. If the Coriolis torque is $\underline{T}_c$ and the chamber surfaces apply torque $\underline{T}_s$, the flow rate of angular momentum at the exit must be

$$\underline{T}_{out} = \underline{T}_{in} + \underline{T}_s + \underline{T}_c - \frac{d}{dt}(\underline{P}) \tag{18}$$

If the fluid viscosity is low, we may neglect shear forces, so that chamber surfaces only apply pressure forces, which are normal to the surface. For a spherical chamber, such forces are all directed toward the center of the chamber. It follows that $\underline{T}_s = 0$.

$\underline{T}_{in}$ depends only on inlet geometry, and is not affected by $\underline{\Omega}$. If $\underline{\Omega}$ changes suddenly from one steady value to another, $d(\underline{P})/dt$ will differ from zero for a time on the order of V/Q, the time required to replace the fluid in the chamber. Eventually, however, $\underline{P}$ will assume a new steady value, so that apart from transient effects, $d(\underline{P})/dt = 0$.

If $\underline{\Omega} = 0$, $\underline{T}_c = 0$ so that $\underline{T}_{out} = (\underline{T}_{out})_o = \underline{T}_{in}$. For $\underline{\Omega} \neq 0$, we have $\underline{T}_{out} = \underline{T}_{in} + \underline{T}_c$ so that

$$\underline{T}_{out} = (\underline{T}_{out})_o + \underline{P} \times \underline{\Omega} \tag{19}$$

With the coordinate system of Figure 10, and unit vectors $\underline{i}$, $\underline{j}$, $\underline{k}$, we have

$$(\underline{T}_{out})_o = \underline{i}\, T_{in} \tag{20}$$

$$\underline{P} = \underline{i}\, P_x \tag{21}$$

$$\underline{\Omega} = \underline{k}\,\Omega \tag{22}$$

$$\underline{P}\times\underline{\Omega} = -\underline{j}\,P_x\Omega \tag{23}$$

Then

$$\underline{T_{out}} = \underline{i}\,T_{in} - \underline{j}P_x\Omega \tag{24}$$

The term $-\underline{j}P_x\,\Omega$ indicates that the outflow direction deviates from the x-direction.

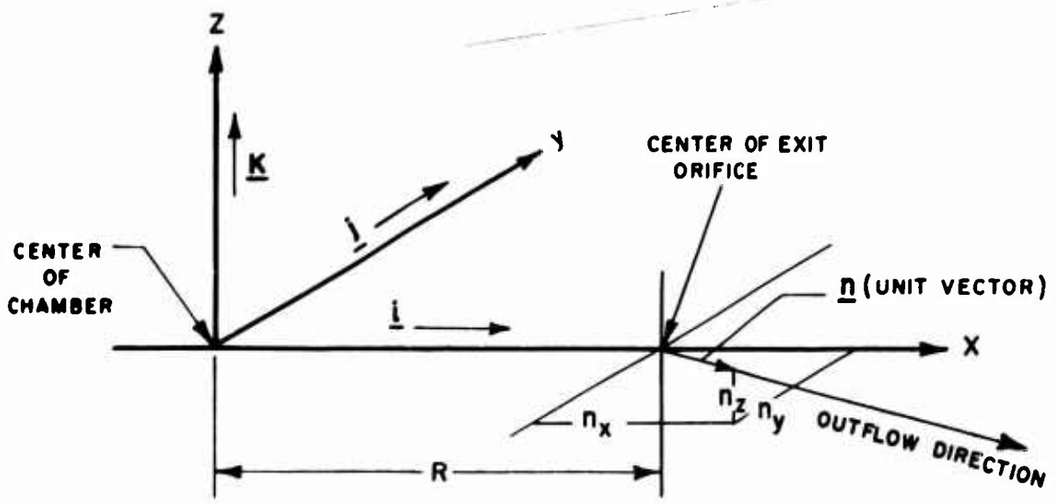

Figure 10. Outflow From Swirl Chamber.

Let $\underline{n}$ be the unit vector in the direction of the outflowing stream of speed W. The linear momentum flow rate of the outflow is $\underline{n}\rho QW/g$, and this is directed through the center of the exit orifice, the location being given by the vector $\underline{R} = \underline{i}R$ drawn from the center of the chamber.

This results in a contribution $(\underline{R}) \times (\underline{n}\rho QW/g)$ to the outflow angular momentum flow rate, $\underline{T_{out}}$.

The magnitude of the angular momentum due to rotation of the outflowing jet about its own axis is T_o, contributing $\underline{n}\,T_o$ to $\underline{T_{out}}$. The sum of these contributions is $\underline{T_{out}}$, so that

$$\underline{i}\,T_{in} - \underline{j}\,P_x\Omega = (\underline{i} \times \underline{n})\,\frac{R\rho QW}{g} + \underline{n}\,T_o \tag{25}$$

Let $\underline{n} = \underline{i}\,n_x + \underline{j}\,n_y + \underline{k}\,n_z$

Then

$$\underline{i}\, T_{in} - \underline{j}\, P_x\Omega = \underline{k}\, n_y \frac{R\rho QW}{g} - \underline{j}\, n_z \frac{R\rho QW}{g} + \underline{i}\, n_x T_o + \underline{j}\, n_y T_o + \underline{k}\, n_z T_o \tag{26}$$

The individual components of this equation are

$$T_{in} = n_x T_o \tag{27}$$

$$-P_x\Omega = -n_z \frac{R\rho QW}{g} + n_y T_o \tag{28}$$

$$0 = n_y \frac{R\rho QW}{g} + n_z T_o \tag{29}$$

where $n_x^2 + n_y^2 + n_z^2 = 1$ since $\underline{n}$ is a unit vector. (30)

Solving the first three of the last four equations for n_x, n_y, and n_z, the fourth equation becomes a quadratic equation in T_o^2, so that n_x, n_y, n_z, and T_o are easily solved for exactly.

For small Ω, we then find the following approximate solutions:

$$T_o = T_{in} \tag{31}$$

$$n_x = 1 \tag{32}$$

$$n_y = -\frac{P_x\Omega}{\left(\frac{R\rho QW}{g}\right)^2 + T_{in}^2} T_{in} \tag{33}$$

$$n_z = \frac{P_x\Omega}{\left(\frac{R\rho QW}{g}\right)^2 + T_{in}^2} \left(\frac{R\rho QW}{g}\right) \tag{34}$$

Let $\tau = V/Q$, the time required to replace the fluid in the chamber. Let R be the chamber radius and V_R the inlet velocity.

Then

$$T_{in} = \frac{\rho}{g} V_R RQ \text{ and } P_x = T_{in}\, \tau \tag{35}$$

and

$$n_y = -\frac{\Omega\tau}{\left(\frac{W}{V_R}\right)^2 + 1} \qquad n_z = \frac{\Omega\tau}{\left(\frac{W}{V_R}\right)^2 + 1} \frac{W}{V_R} \tag{36}$$

The $\underline{n}\ \underline{i}$ plane determined by the outflow direction and the x-axis is tilted with respect to the xy plane through an angle $\tan^{-1}(n_z/n_y)$. In the $\underline{n}\ \underline{i}$ plane, the outflow direction makes angle $\sin^{-1}(n_y^2 + n_z^2)^{1/2}$ with respect to the x-axis. This angle is a maximum when $W<<V_R$, the angle then being $\Omega\tau$ (for small $\Omega\tau$). If $W = V_R$, the angle is reduced to $\Omega\tau/\sqrt{2}$.

The deflection of the emerging jet by an angle on the order of $\Omega\tau$ should be readily detectable by a pair of pressure sensors symmetrically placed along the axis of the jet. The distance through which the jet is deflected will be the product of the angle and the distance L' from the exit orifice to the pressure sensors. This will cause a delay $\tau' = L'/W$. By making V_R and W large enough, τ' can be made small. This is an advantage over the usual jet-type rate sensor in which the deflection distance would be $\Omega\tau'L'$.

One problem has to be solved before the foregoing theoretical design can be put into practice; namely, the emerging jet tends to cavitate because of its rapid rotation.

CORIOLIS PRESSURE GRADIENT DEVICE

In Figure 11, let v be the tangential flow velocity in the annular swirl chamber. The angular momentum of the fluid is

$$P_x = \left(\frac{\rho}{g} vR\right) (2\pi RL \Delta R) \tag{37}$$

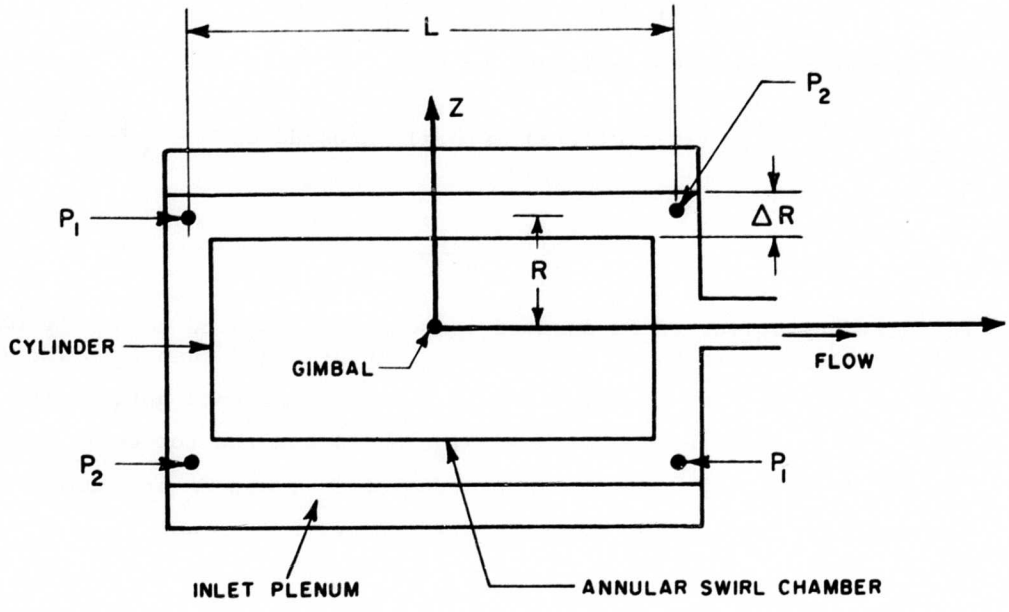

Figure 11. Coriolis Pressure Gradient Device.

With angular velocity of the rotating coordinate system Ω about the z-axis, the Coriolis torque about the y-axis (into the paper) is

$$T_c = - P_x \Omega \tag{38}$$

Neglecting the end clearances between inner cylinder and housing, and considering the inner cylinder and housing to be rigidly connected, the torque T_c must be due to the pressure distribution on the annular areas on the end faces, with radial dimension ΔR.

The maximum and minimum pressures P_1 and P_2 differ by

$$P_1 - P_2 = 2 \frac{\rho}{g} vL\Omega \tag{39}$$

The inner cylinder has a pressure distribution on its surface. If the inner cylinder is now made free to rotate about the y-axis, and is restrained by the torque-measuring system discussed earlier in connection with Figure 8, the pressure distribution will generate a torque which we will now derive:

Select cylindrical coordinates θ and x with $\theta = 0$ in the z-direction. Let $P(\theta,x)$ be the pressure on the surface of the inner cylinder at coordinates θ and x. Then, because of the Coriolis pressure gradient,

$$P(\theta, -x) - P(\theta,x) = \frac{4\rho v\Omega x}{g} \cos\theta \tag{40}$$

The torque on the inner cylinder is then

$$T_{cyl} = -\int_o^{L/2} \int_o^{2\pi} (2x)\cdot(P(\theta,-x) - P(\theta,x)) R\cos\theta d\theta\, dx = -\frac{\pi}{3} \frac{\rho v\Omega R L^3}{g} \tag{41}$$

$$\frac{T_{cyl}}{T_c} = \frac{L^2}{6R\ \Delta R} \tag{42}$$

In this derivation, ΔR is assumed to be small compared to R. By making L large compared to R, we can make T_{cyl} much larger than T_c. The reason for this is that in magnitude T_c is the difference between the magnitude of T_{cyl} (counterclockwise in Figure 11) and the torque T_h on the housing (clockwise). If the magnitudes of T_{cyl} and T_h are nearly equal, each must be much larger than the difference.

EXPERIMENTS WITH SWIRL CHAMBER

Experiments were performed with the swirl chamber (shown in Figure 12) installed in the water tank. Some aluminum parts were pitted during the experiments. Component parts are shown in Figure 13. The outside diameter of the outer chamber is 6-1/4 inches, the inside diameter of the inner chamber (upper right in Figure 13) is 3 inches and the inside length is 5 inches.

The front and back ends were similar, so that the inserts shown in Figure 14 could be installed at either end. The insert installed in the back end in the first experiments is not shown. It contained a pair of small pressure-sensing holes separated by 1/8 inch straddling the chamber axis, and connected to manometers with air over the free surfaces of the water to permit differential pressure changes to be read. The front end contained the lower right insert shown in Figure 14. At most, a small differential pressure change was observed when the swirl chamber was rotated about a vertical axis.

Two explanations for this observation seemed to be possible:

1. The hollow space along the axis due to cavitation, which was clearly visible, extended beyond the pressure-sensing hole.
2. The orientation of the flow axis is "clamped." That is, it cannot rotate because it must pass through the center of the chamber, as well as through the center of the exit hole.

To test these explanations, we replaced the exit hole with the off-center hole and with the small hole (lower left and upper right in Figure 14). The off-center hole tilted the flow axis and yielded a pressure differential. The small centered hole raised the pressure inside the chamber and reduced the diameter of the cylindrical cavitation, but a substantial pressure differential did not result when the swirl chamber was rotated.

The lower insert in Figure 14 is a slot with slightly off-center pressure taps. This was tried to see whether rotation of the swirl chamber might cause the flow axis to shift along the slot. No appreciable effect was observed, however. This was attributed to very stable centering of the flow through the center of the slot.

The upper and the upper left inserts in Figure 14 were then tried on the basis that with two exits, the flow would be less stably centered and more responsive to disturbances tending to shift the flow axis. Pressures were read from the taps 1/8 inch apart at the back end of the chamber. With the larger pair of holes, no response was found when the swirl chamber was rotated. With the smaller pair, the flow axis tended to oscillate between the two holes, producing a pulsating output at the pressure taps.

This observation encouraged the view that a suitably shaped exit orifice would be nearly neutral in regard to the orientation stability of the

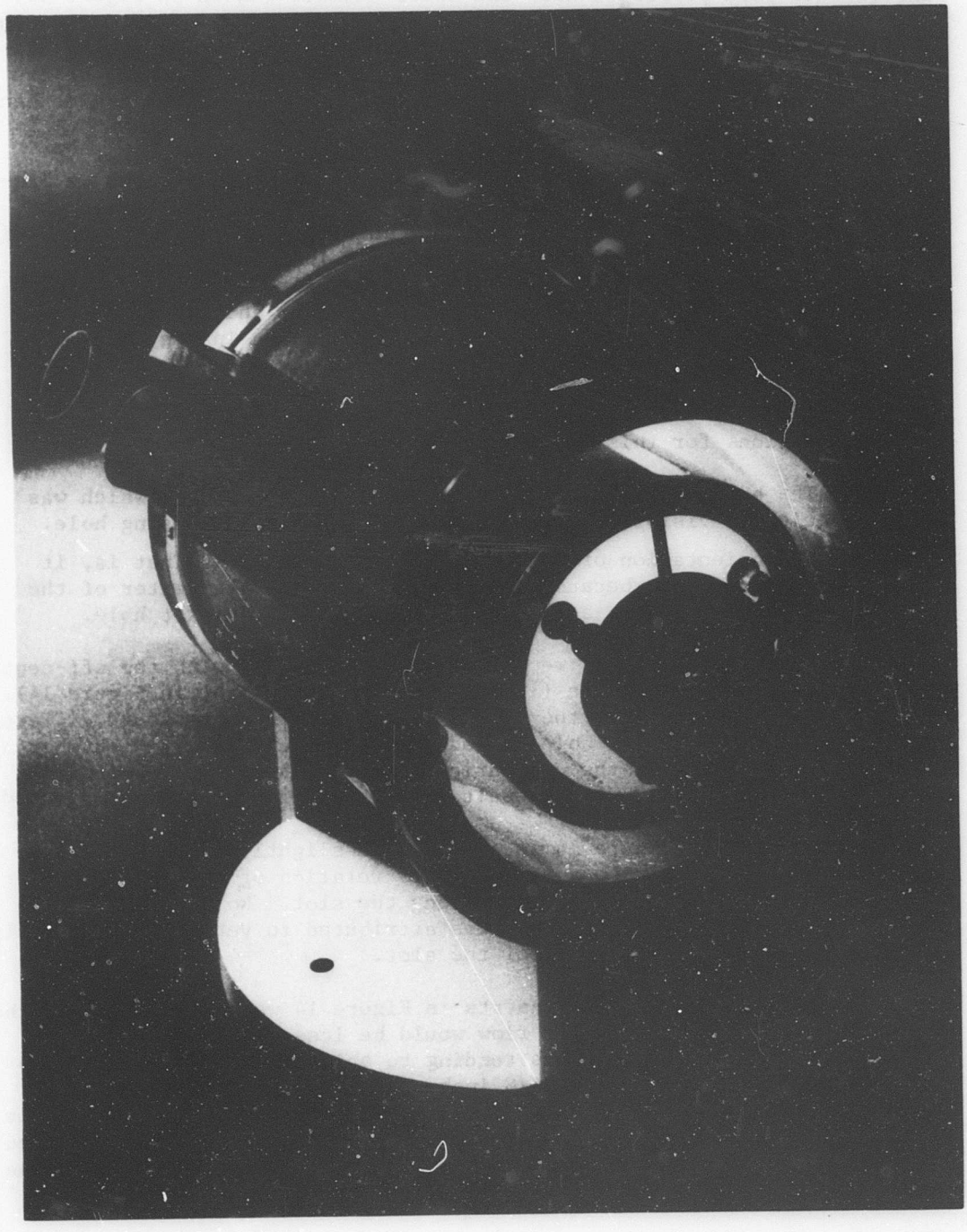

Figure 12. Swirl Chamber.

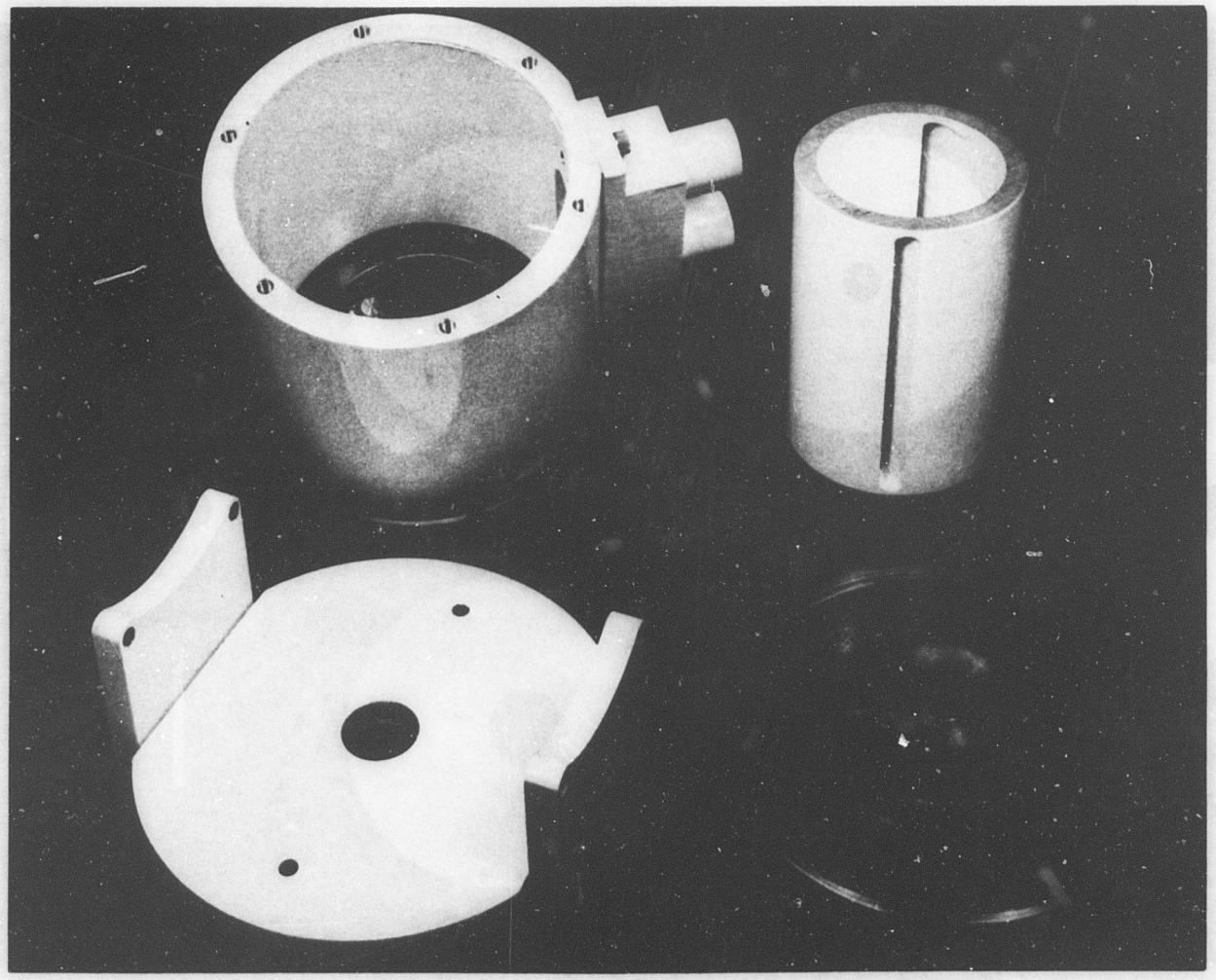

Figure 13. Swirl Chamber Parts.

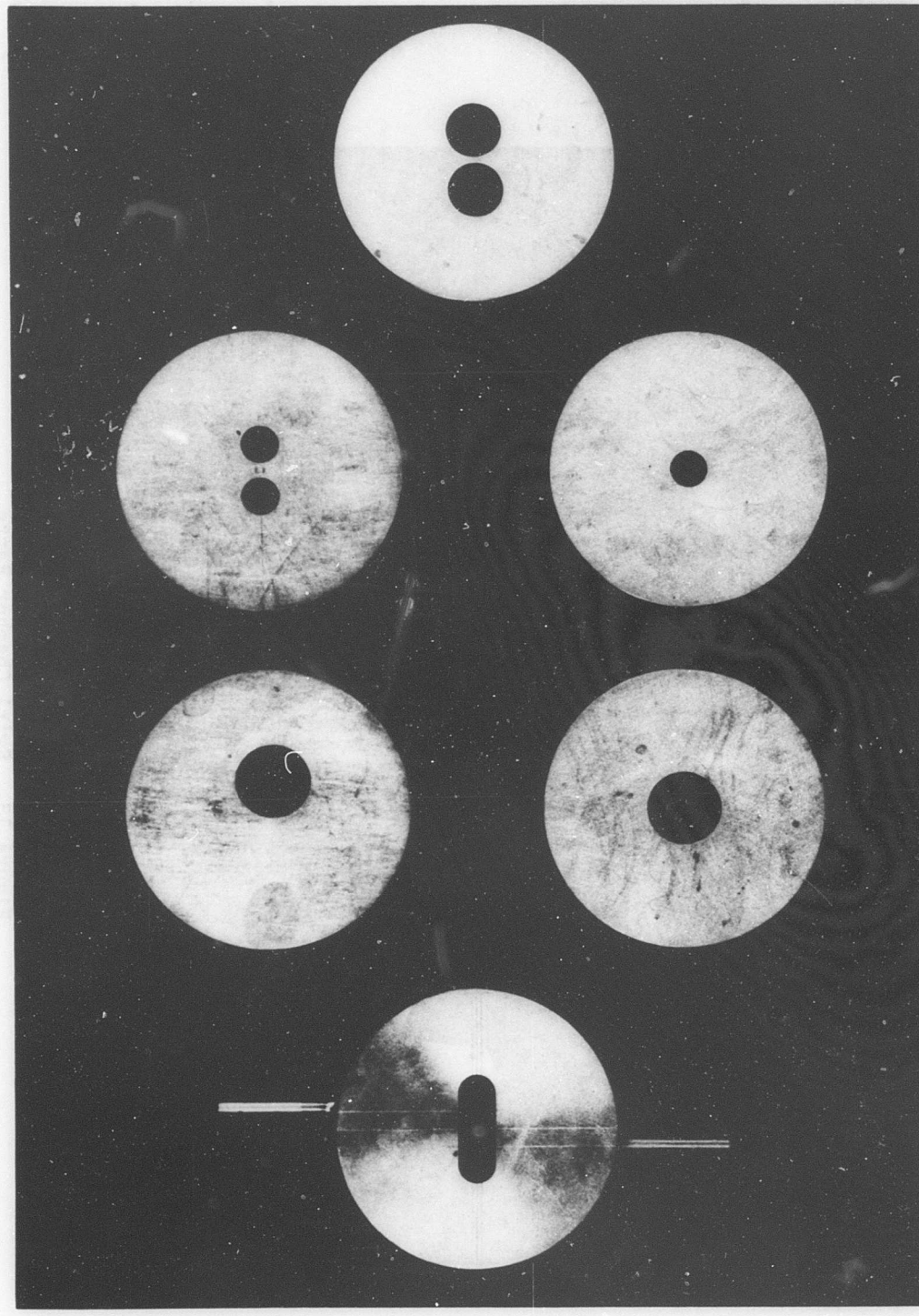

Figure 14. Swirl Chamber Inserts.

flow axis. Accordingly, the figure-eight orifice shown in Figures 12 and 13 was tried. One of the pressure taps is visible in Figure 12 just above the narrow waist of the orifice. The other tap is symmetrically located just below the waist. A pressure difference of several inches of water was observed between these taps when the swirl chamber was rotated.

Various visual observations were made on the cavitation region, which clearly marks the flow axis. In one observation, the off-center orifice, was used at the front of the swirl chamber and the small centered orifice was used at the back.

As viewed from the front, the swirl was clockwise. With the off-center hole at "six o'clock," the cavitation region was curved, approximately planar, going upward and to the right at about "two o'clock" from the exit hole.

The curvature of the flow axis, and the fact that it did not lie in the plane defined by the center of the cavity and the centers of the exit holes, suggested that greater sensitivity to rotation of the chamber might be found either with the pressure taps located near the center of the chamber rather than the end face, or with the exit port at the center of the chamber. Either of these would require connections to the center of the chamber, which might interfere with the swirl flow. A good deal of effort was spent in an attempt to develop a theoretical understanding of the shape of the flow axis, but the problem has not been solved.

After the observations with the swirl chamber in the water tank, the swirl chamber was transferred to the rate table, as shown in Figure 4. Two pressure transducers were provided, one for each output port of the figure-eight orifice. Unfortunately, because of damage to one of the pressure transducers, only one transducer was usable. It was attached to one of the output taps of the figure-eight orifice. With maximum available flow through the chamber, a small signal was obtained when the rate table was rotated rapidly (about 7 deg/sec). The figure-eight orifice was then modified by smoothing all sharp edges. Substantial signals were obtained with various rotation rates; however, the signals were very noisy. With electronic filtering to remove high-frequency components, the output trace shown in Figure 15 was obtained by switching back and forth between the two directions of rotation of the rate table.

In view of the slow response (due to the filtering) and the high rate-table speed, the signal-to-noise ratio appears to be smaller than ultimately desired, by a factor on the order of 2000. Nevertheless, the principle of the method of angular rate measurement has been clearly demonstrated.

The figure-eight orifice was then replaced by the orifice probe shown in Figure 16. Flow is from left to right. Only a small part of the flow is supposed to exit through the axial tube. Most of the flow

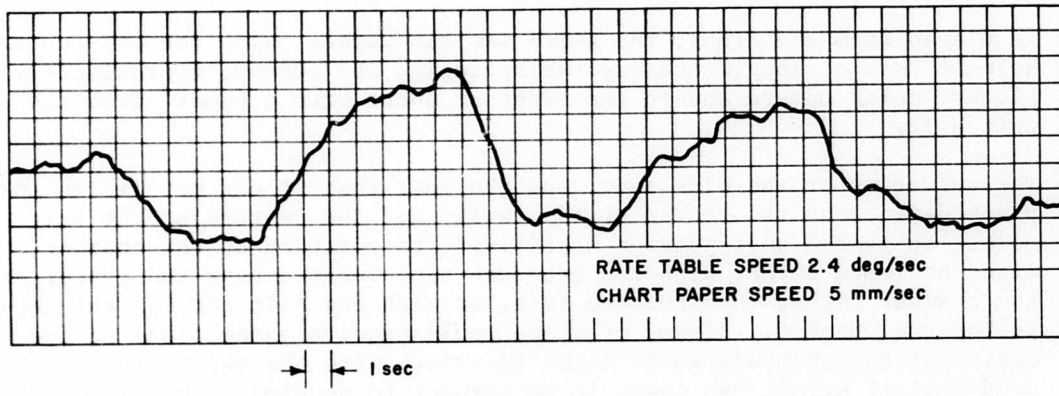

Figure 15. Electronically Filtered Output Trace With Figure-Eight Orifice.

should leave through the banana-shaped slots surrounding the base of the tube. The purpose of this design was to minimize the "clamping" effect that the exit design has on the swirl flow axis. Initial observations were not substantially better than those with the figure-eight orifice, but after some rounding of the conical entrance where it joins the cylindrical exit passage, a much larger output signal was obtained, with about ten times as much sensitivity as that obtained with the figure-eight orifice. Here sensitivity is to be understood as follows: with the rate table turning at a given speed, its direction of rotation is reversed. The output signal then requires some time to shift to a new equilibrium value. The signal-to-noise ratio divided by the product of time required for the shift times the angular rate is taken as a measure of sensitivity. In contrast to the figure-eight orifice which yielded a sensitivity that was lower than that ultimately desired by a factor of about 2000, the corresponding factor with the orifice probe was about 200.

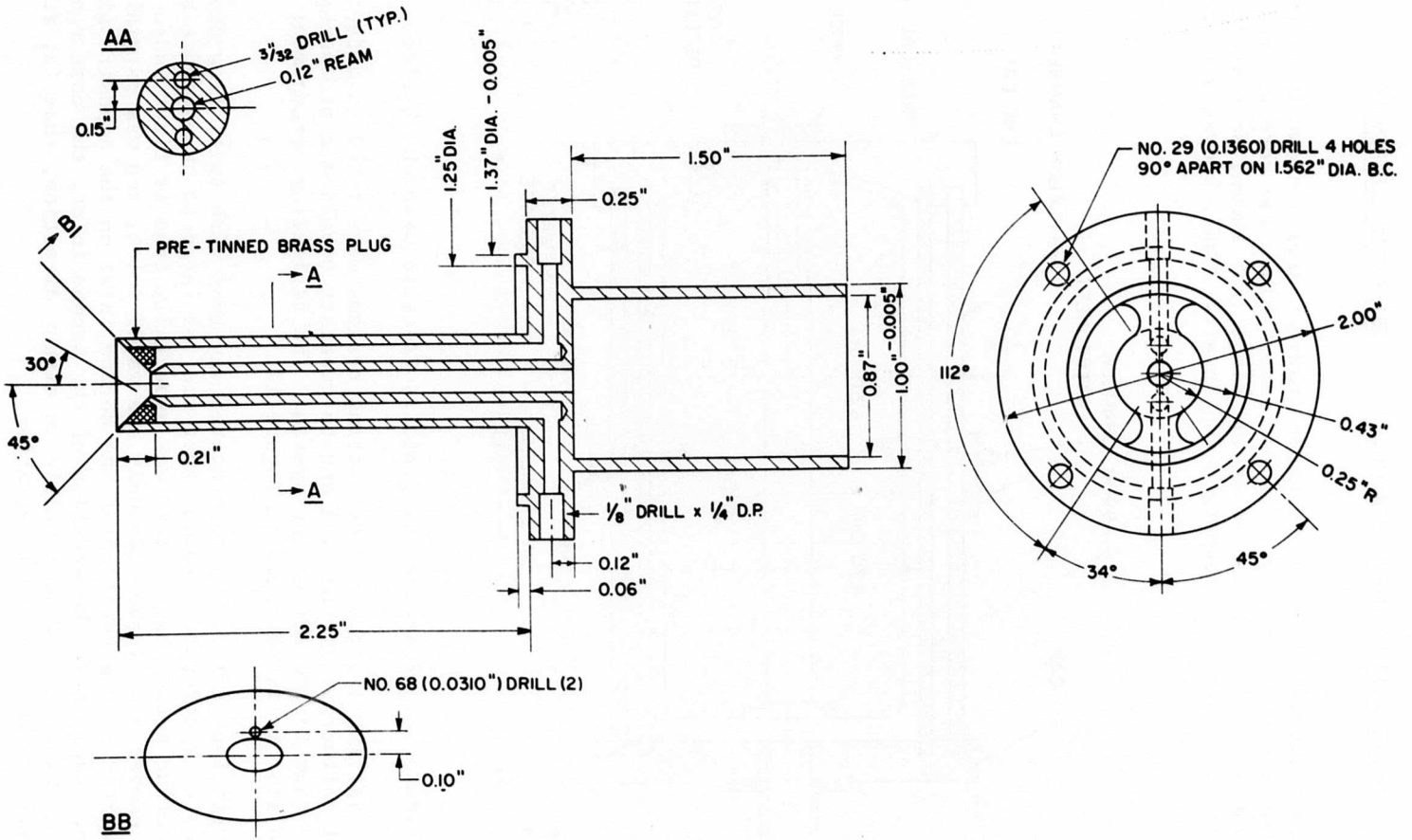

Figure 16. Orifice Probe.

OBSERVATIONS WITH CORIOLIS PRESSURE GRADIENT DEVICE

The experimental Coriolis pressure gradient device shown in Figure 17 was constructed and mounted on the rate table. The core was made of nylon and was provided with balancing slugs (not shown) so that it could be balanced both when submerged and in air. Thus, buoyancy forces should not create any torque.

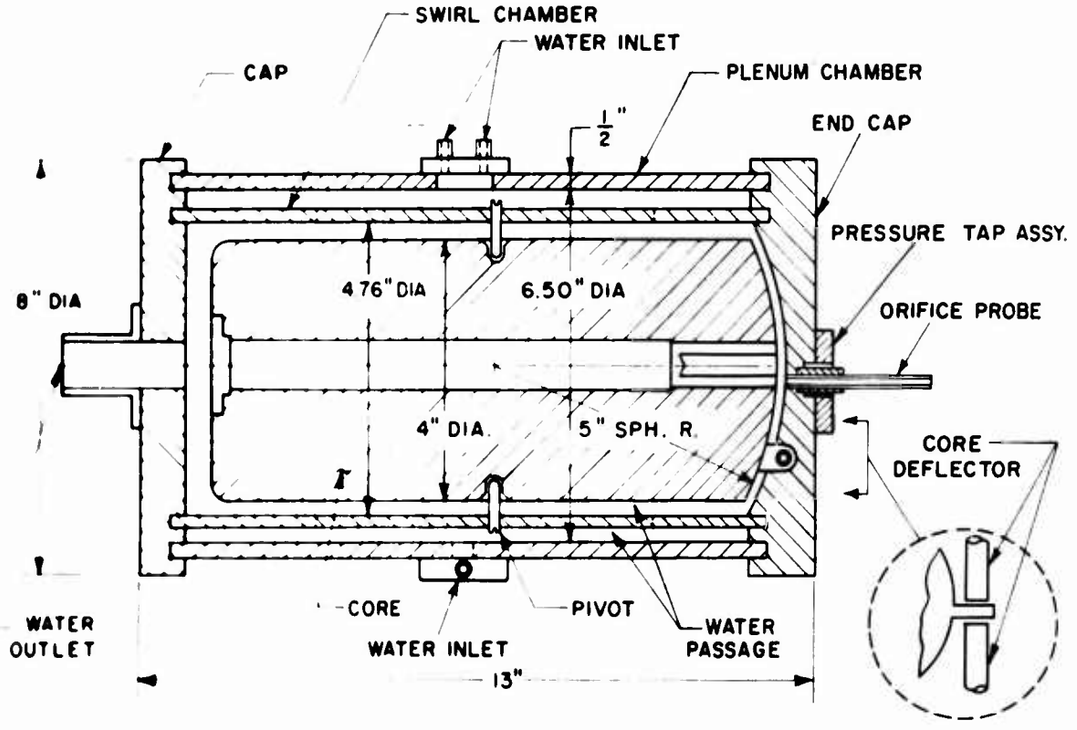

Figure 17. Experimental Coriolis Pressure Gradient Device.

A few valving systems and deflecting systems were tried to detect the small deflection of the core and to generate unbalanced pressures and apply them to the deflecting system. The deflecting arrangement that was tried last is illustrated in Figure 17.

The principal difficulty encountered was that with swirl flow present, the core experienced a torque that was too large to be overcome by the deflecting arrangement. This was especially true at first, when the plenum chamber was fitted with only one water inlet, and was partially alleviated by the addition of the second inlet on the opposite side, as shown. Even after the addition of the second inlet, the core tended to remain tilted as far as possible in either direction; that is, it was bistable rather than self-centering.

It appeared, therefore, that the valving arrangement and the core deflector must constitute a circuit with sufficient gain to overcome the instability of the core in its centered position. The core deflector arrangement shown in Figure 17 appeared to accomplish this. However, the pressure in one leg of the core deflector was extremely noisy when observed by the pressure transducer and strip chart recorder. The noise masked any signal that may have been generated when the rate table was operated.

The severe noise is attributed to the inlet design, which is probably conducive to turbulence. It would seem desirable to enlarge the plenum chamber and provide smooth turns for the inlet flow. However, time and funds did not permit pursuing this further.

CONCLUSIONS

Several concepts have been considered for using vortex flow in an angular rate sensor. Experiments were performed with some of them using a water tank and a simple rate table.

The concept of the vortex axis jet angular rate sensor (VAJARS), in which the inner of two concentric jets is rapidly rotated, led to experiments with concentric vortex chambers in the water tank. With the aid of flow visualization, it was found that the inner (axial) jet of the VAJARS did not have sufficient rotational speed, and that turbulence appeared to be a disturbing factor as well. The outer jet could be made to rotate more rapidly, but this caused cavitation and flow reversal along the axis.

A swirl chamber was tested with various exit orifice designs. The first successful orifice was the figure-eight design and the next successful orifice was the orifice probe. These are described in the body of the report, and led to sensitivities that were lower than ultimately desired by factors on the order of 2000 and 200, respectively; however, the principle of the device was successfully demonstrated.

The theory of the swirl chamber is that the axis of the swirl flow lags behind the axis of the chamber when the chamber is subjected to an angular rate about another axis, and theoretically, the desired sensitivity is achievable. A theoretical examination of two-dimensional swirl flow shows that with sufficiently high Reynolds number, viscous shear forces have a negligible effect on velocity distribution.

Theoretical discussion is also given for two additional concepts: a gyroscope in which the rotor is a fluid, and a swirl chamber supplying an external jet, the deflection of which is proportional to the angular rate and the time it takes for the inlet flow to replace the fluid in the swirl chamber.

Finally, the pressure gradient generated in an annular swirl chamber by Coriolis forces is the basis for a "moving parts" device with high theoretical sensitivity. Brief experimental efforts encountered difficulties that could not be ironed out in the remaining time; namely, an instability in the positioning of the moving part and noise due to turbulence in the flow. However, these are not difficulties in principle and it should be possible to overcome them.

It was shown experimentally that a very sensitive flow velocity probe can be made, based on the iodine-iodide redox system. The probe sensitivity was an order of magnitude greater than would have been useful in the present study.

LITERATURE CITED

1. G. P. Wachtell, FEASIBILITY OF A TOROIDAL STREAM ANGULAR RATE SENSOR, The Franklin Institute Research Laboratories, USAAVLABS Technical Report 68-11, U. S. Army Materiel Laboratories, Fort Eustis, Virginia, April 1968, AD 671 023.

2. P. M. W. Navé , Acta Physica Austria ca 22, 1966, 259-264.

Unclassified

Security Classification

DOCUMENT CONTROL DATA - R & D

(Security classification of title, body of abstract and indexing annotation must be entered when the overall report is classified)

1. ORIGINATING ACTIVITY (Corporate author) The Franklin Institute Research Laboratories 20th and Race Streets Philadelphia, Pennsylvania	2a. REPORT SECURITY CLASSIFICATION Unclassified 2b. GROUP

3. REPORT TITLE

FLUIDIC VORTEX ANGULAR RATE SENSOR CONCEPT INVESTIGATION FOR HELICOPTERS AND V/STOL AIRCRAFT

4. DESCRIPTIVE NOTES (Type of report and inclusive dates)

Final Report

5. AUTHOR(S) (First name, middle initial, last name)

G. P. Wachtell

6. REPORT DATE April 1970	7a. TOTAL NO. OF PAGES 44	7b. NO. OF REFS 2
8a. CONTRACT OR GRANT NO. DAAJ02-69-C-0010 new b. PROJECT NO. Task 1F162203A14186 c. d.	9a. ORIGINATOR'S REPORT NUMBER(S) USAAVLABS Technical Report 70-25 9b. OTHER REPORT NO(S) (Any other numbers that may be assigned this report)	

10. DISTRIBUTION STATEMENT

This document is subject to special export controls, and each transmittal to foreign governments or foreign nationals may be made only with prior approval of U. S. Army Aviation Materiel Laboratories, Fort Eustis, Virginia 23604.

11. SUPPLEMENTARY NOTES	12. SPONSORING MILITARY ACTIVITY U.S. Army Aviation Materiel Laboratories Fort Eustis, Virginia

13. ABSTRACT

An experimental investigation was undertaken to establish the feasibility of using fluidic vortex angular rate sensors in helicopter and V/STOL aircraft stability augmentation systems. Theories of various possible rate sensing devices based on rapid vortex flows are presented, with experimental demonstration of the principle of one in which the swirl flow axis lags behind the chamber axis when the chamber is rotated about a line perpendicular to its axis. Two modifications yielded sensitivities less than ultimately desired by factors on the order of 2000 and 200. Observations on the flow pattern in jets emerging from a pair of concentric vortex chambers showed that the concept of the vortex axis jet angular rate sensor (VAJARS) would have to overcome problems created by turbulence and flow reversal along the axis. An attempt was made to demonstrate a device of high theoretical sensitivity, in which a cylindrical core supported on an axis perpendicular to the core axis is subjected to a torque due to the pressure gradient generated in an annular passage by Coriolis forces. The problem of noise due to turbulence, as well as instability in the position of the core, was believed to be possible to overcome. Theoretical discussions are also given of a gyroscope in which the fluid stream is the rotor, and of the deflection of the jet emerging from a swirl chamber subjected to an angular rate. A flow rate sensor based on the iodine-iodide redox system was demonstrated in an attempt to develop a velocity probe. Sensitivity was an order of magnitude too high for the present flow studies.

DD FORM 1 NOV 68 1473 REPLACES DD FORM 1473, 1 JAN 64, WHICH IS OBSOLETE FOR ARMY USE.

Unclassified

Security Classification

14. KEY WORDS	LINK A		LINK B		LINK C	
	ROLE	WT	ROLE	WT	ROLE	WT
Vortex axis jet angular rate sensor (VAJARS)						
Helicopter						
V/STOL aircraft						
Vortex chamber						
Gyro rotor						
Fluid gyro						
Coriolis pressure gradient device						